REGULAR ARTICLE

Computational studies of the interactions of I^- and I_3^- with TiO$_2$ clusters: implications for dye-sensitized solar cells

Abu Md. Asaduzzaman · Georg Schreckenbach

Abstract First principle density-functional theory calculations have been carried out on the interaction of I^- and I_3^- with TiO$_2$ anatase surfaces, modeled by finite clusters that range in size from 48 to 180 atoms. The total energy per TiO$_2$ unit and the HOMO-LUMO gaps decrease with increasing the size of the clusters. Both redox species (I^- and I_3^-) are strongly adsorbed on the TiO$_2$ surface with the adsorbtion of I^- being stronger. Adsorption of triiodide leads to its dissociation. The positions of the HOMO and LUMO of the adsorbed systems shift negatively from their respective cluster values. Solvation effects have been modeled using the CPCM model. Introducing solvent reduces the shifting of HOMO and LUMO. Implications for dye-sensitized solar cells (DSSC) are discussed. Both the HOMO-LUMO shifting and the strong adsorption might affect the performance of the cell.

Keywords Iodide · Dye-sensitized solar cell (DSSC) · Density functional theory (DFT) · Anatase · Cluster calculations · Adsorption

1 Introduction

Solar energy conversion by photo-electrochemical devices is being intensely investigated as an alternative energy source to conventional fossil-fuel based energy systems [1–8]. Of the several different types of next-generation solar cells under development, the dye-sensitized solar cells (DSSC) have attracted considerable interest because of high photo conversion ability, easy processing and low-cost materials [9–13].

Since the first report of a high conversion efficiency for a dye-sensitized TiO$_2$-based solar cell by Grätzel and O'Regan in [14], there has been an intense interest in understanding the elements that control the efficiency and performance of the cell. To date, an energy conversion efficiency of about 11% has been achieved for regenerative photo electrochemical cells based on nanocrystalline TiO$_2$ with the sensitizer cis-Ru[(4,4′-COOH)$_2$-2,2′bipyridine]$_2$ (NCS)$_2$, known as the N3 dye, and its derivatives [10, 15–20], and an I^-/I_3^- redox couple in an organic solvent.

A typical DSSC has three main components: (1) At the heart of the cell is a mesoporous oxide layer composed of nanometer-size semiconductor particles. Usually TiO$_2$ is used as the semiconductor. A monolayer of photo-excitable dye is attached to the surface of the semiconductor. The remaining two components are (2) an electrolyte solution containing a redox couple (usually an organic solvent containing the I^-/I_3^- couple), as well as various additives [21], and (3) a counter electrode to complete the circuit. Current research efforts in developing and/or understanding the DSSC tend to be focused mainly on the development of new dyes with an absorbance profile that better matches the solar spectrum [12, 20, 22–24], methods to increase the operating voltage in the open circuit setting [11, 13, 25–27], dye regeneration processes [28, 29], searching for an alternative redox couple [30–32], etc. The operation of a DSSC is a complex multi-step physico-chemical process. A problem in any single step may cause a drastic change in the overall performance of the cell.

A. Md. Asaduzzaman · G. Schreckenbach (✉)
Department of Chemistry, University of Manitoba,
Winnipeg, MB R3T 2N2, Canada
e-mail: schrecke@cc.umanitoba.ca

In a DSSC, charge separation occurs in the adsorbed dye by the injection of photo-excited electrons into the conduction band of the TiO$_2$ electrode and the reduction of the resulting dye cations by I$^-$/I$_3^-$ in the electrolytic solutions. At short-circuit conditions, the electrons and I$_3^-$ diffuse to a transparent conductive oxide and a Pt counter electrode, respectively. The charge collection efficiency depends on the electron diffusion length in the TiO$_2$ semiconductor [33], which is equal to

$$(\text{electron diffusion coefficient} \times \text{electron lifetime in the TiO}_2)^{0.5}$$

If the electron diffusion length is shorter than the thickness of the TiO$_2$ electrode, the electrons in the TiO$_2$ will recombine with the dye cations and/or the I$_3^-$. Therefore, for a DSSC having optimal photon-to-current conversion efficiency, the short-circuit current should be maximal. At open-circuit conditions, the electrons from the excited dye at the TiO$_2$ conduction band will accumulate until the charge injection rate is balanced by the recombination rate. The number of electrons in the TiO$_2$ conduction band is also significant in determining the Fermi level of TiO$_2$, which is directly related to the voltage of the cell.

There are some studies [33, 34] where scientists tried to increase the electron lifetime in the conduction band of TiO$_2$. For DSSCs based on organic dyes, Koumura et al. [34] have done this by adding n-hexyl chains to the thiophene moieties of the dye. The mechanism for increasing the electron lifetime is postulated to be as follows: The authors propose that the redox couple is being blocked by the large tail of the dye from coming close to the TiO$_2$ electrode. Clifford et al. [28] have studied the dye regeneration process with the I$^-$/I$_3^-$ redox couple. They have shown that the regeneration processes progress through the intermediate formation of I$_2^-$. We have applied quantum chemistry to study the dye regeneration mechanism [35, 36] following the work of Clifford et al. Very recently [29], there has been another experimental study on the dye regeneration process of DSSCs. In this article, short-lived iodine atoms were reported as intermediates in the regeneration process. To develop DSSCs with improved performance and efficiency, we must better understand the basic interactions of the redox couple with all the various components of the DSSC.

Although it is established that I$^-$/I$_3^-$ is a unique redox couple for the DSSC and various other species related to the redox couple are formed during their redox reactions [28, 29], there is hardly any attention being paid to understanding the interaction of the redox species with the TiO$_2$ semiconductor, the dye and/or the counter electrode.

We have categorized the interactions of the redox couple in the DSSC in two ways: (a) interactions of the redox species with the semiconductor surface, which might affect the performance of the cell, and (b) interactions with the dye and the counter electrode, which essentially involves the dye regeneration process. Systematic theoretical calculations have been carried out on the interactions of the redox couple with the semiconductor surface and the dye. We have reported the latter part elsewhere [35, 36].

It is worth mentioning that the interactions between the redox couple and the TiO$_2$ surface can be modeled in two different, complementary ways: the cluster model and periodic surface models with different crystallographic orientations. The nanoparticles used in the DSSC have specific crystallographic orientations. The presence of any defects on the surface such as kinks, step edges, oxygen vacancies, etc. plays a role in the electronic properties of TiO$_2$ particles [37]. In the modeling context, the study of such defects is more amenable for surface modelling using periodic boundary conditions but is difficult to achieve for clusters.

The goal of this article is an investigation of the interaction of iodide and triiodide with TiO$_2$ anatase surfaces, and to relate this to the operation of the DSSC. It is clear that the other components present in the cell might influence the TiO$_2$—redox shuttle interactions, however, as a basic study, our study will give us an idea about the possible effects due to this TiO$_2$—redox shuttle interaction. In addition, O'Regan et al. [38] pointed out the importance of the iodine complexation with TiO$_2$ and the dye in the improvement of the cell performance.

In this work, we model the surface using cluster models, as this allows us to directly apply the machinery of molecular quantum chemistry [39]. In particular, we can include the influence of the solvent using continuum solvation models [40–42]. A complementary study using surface modeling has been published elsewhere [43]. Although solvation modeling for periodic calculation is in principle possible, its implementation requires extensive work and thus would warrant a separate project [44, 45].

2 Computational methods

All calculations have been carried out using four different computational packages, namely Priroda (version 5) [46–48], Gaussian (g03) [49], TURBOMOLE [50], and the Amsterdam Density Functional package (ADF) [51–54] in the framework of density functional theory (DFT). The exchange and correlation functional is treated with the approximation due to Perdew, Burke and Ernzerhoff (PBE) [55] in both Priroda and g03. Earlier, we have reported [56] that pure GGA functionals such as PBE nicely estimate the energetics and structures of various small iodine species. Moreover, we have shown the implementations of

approximate DFT to be entirely comparable between Priroda and g03, provided that sufficiently converged basis sets are used [57, 58].

Geometries have been fully optimized with Priroda in the gas phase. Frequency calculations have been used to verify that true local minima have been obtained in each case. Only single point energies have been calculated with g03 on the Priroda optimized geometries, both in the gas phase and in acetonitrile (CH₃CN) solvent using the conductor polarizable continuum model (CPCM) [40]. Continuum solvation models such as CPCM contain empirical parameters [41, 42]. For that reason, the results depend critically on the choice of parameters, notably the size of the solvent-excluded cavity (atomic radii). Previously, we [58] and others [59] have found that CPCM is a reasonable choice in this respect. Moreover, we are particularly interested in qualitative trends between gas phase and solution, which puts less stringent requirements on the accuracy of the solvation model than would, for instance, the calculation of absolute energetics. The dispersion energy is calculated using Grimme's [60, 61] latest dispersion correction scheme as implemented in the ADF2010 (DFT-D3). Fully relativistic calculations have been carried out as single point energy at the Priroda optimized geometry using the PBE-D3 functional. Basis-set superposition error (BSSE) calculations have been carried out using the TURBOMOLE [50] code at the Priroda optimized geometries for the smaller clusters with PBE functional and double zeta basis sets similar to those of Priroda. The calculated BSSE for both I^- and I_3^- is small (0.10 and 0.14 eV, respectively for the 48 atom cluster) and therefore not included in the discussion. A single point energy calculation using the PBE0 [62] hybrid functional has also been carried out using the TURBOMOLE code using the same basis set for the smaller systems. The trends of the adsorption energy for I^- and I_3^- and the charges are very much similar to those obtained by Priroda and hence only the results obtained by Priroda are presented in Sect. 3.

Priroda applied a four component scalar relativistic method where spin–orbit effects were projected out and neglected [63]. All electron correlation consistent double zeta basis sets with one polarization function have been employed for the large component, with the corresponding kinetically balanced basis sets for the small component [48]. For g03 calculations, we have used the 6-31+G(p) basis set for O atoms and the Stuttgart-Dresden basis sets for the Ti [64] and I [65] atoms. The use of relativistic effective core potentials ensures that (scalar) relativistic effects arising from the presence of the Ti and I atoms are treated. Adding one more diffuse function to the O atoms for the negatively charged system changes insignificantly the energy of frontier orbitals in the g03 solvation calculations. In ADF calculations, relativistic effects

are treated using the Zeroth Order Regular Approximation (ZORA) to the Dirac equation with spin–orbit operator [66, 67]. The PBE functional in conjunction with the ZORA-TZP basis sets for all atoms are employed. The SV(P) [68] basis set is used in the TURBOMOLE code.

The structure of TiO₂ has been modeled using the cluster model. We should emphasize that we use finite clusters as models for the TiO₂ surface, and not for the (much larger) nanoparticles that are employed in DSSCs. As mentioned already, this allows us to use continuum solvation models in a straightforward manner. Clusters are generated from the anatase phase [69] of TiO₂. In generating clusters, two characteristics are always met. (1) The minimum coordination number for oxygen is 2 and that for Ti is 5, and (2) we are always keeping the 1:2 stoichiometry for Ti and O. In this way, we have avoided any unwanted energy states that might influence the results. (These states are unwanted in the sense of surface modeling.) It is worth to mention that we have not kept any fixed orientation while generating the clusters. Instead, starting from a big supercell of the bulk, we have generated spherical-type clusters.

The number of atoms in the calculations varies from 48 to 180 atoms. As an example, the optimized structure of the 138-atom cluster is shown Fig. 1. Pictures of other optimized geometries and the coordinates of the optimized systems can be found in the electronic supplementary information. Given the system size and computational methods, the study of clusters larger than 180 atoms is beyond our scope, although, as mentioned, nanoparticles used in actual DSSCs are much larger. However, we believe that the results obtained in the current study are applicable and/or can be extrapolated to larger particles of TiO₂.
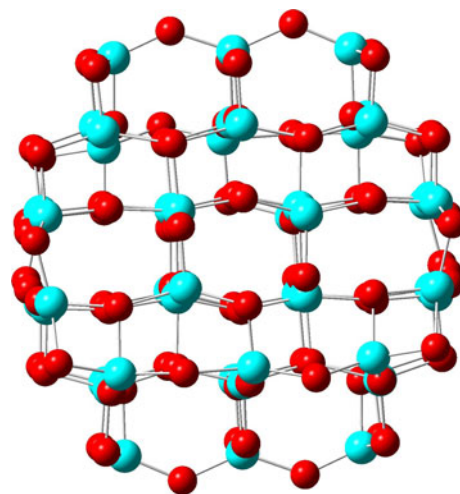

Fig. 1 Optimized structure of the 138-atom cluster. *Red* and *blue* spheres represent O and Ti atoms, respectively

Since we have considered spherical clusters, with increasing the size of the cluster, the number of atoms in the xy-plane (considering z as being normal to the surface) and the thickness in the z direction are increasing. In addition, the minimum coordination number of O and Ti in the bulk TiO_2 are 2 and 5, respectively, which are the same as for the clusters in this study (as already mentioned). Therefore, we would expect convergence of our cluster calculations with respect to an infinite surface. In fact, we have obtained several properties like, for instance, the Ti–I bond distance, the shifting of frontier orbitals, or the adsorption of pyridine and related small molecules (not shown here) that are all well converged (see Sect. 3) with respect to previous periodic surface calculations [43], giving confidence in the cluster calculations. In order to further evaluate the cluster model, we have also checked the trends of the total energy and density of states (DOS) with respect to the size of clusters. Both of them change gradually and are close to convergence. In addition, the adsorption properties of the redox shuttle and small organic molecules (not presented in this article) on clusters also converge to bulk [43], which gives us additional confidence in our cluster model.

3 Results and discussions

All structures are optimized at their local energy minima. In the optimization process, atoms from the surfaces of the clusters were rearranged to minimize the bonding of the surface atoms. On the other hand, the inner parts of the clusters have not changed significantly and retain their bulk configuration.

The relative stability of the different clusters has been extracted from their relative energies. The total energy has been divided by the number of TiO_2 units in the respective clusters. The lowest energy/per unit is considered as zero. Based on that, we have obtained the relative energies per unit for the other clusters. Figure 2 shows the relative energy with respect to the number of TiO_2 units.

From this figure, it is clear that the relative energy is decreasing with increasing the number of TiO_2 units. This observation can be understood from the fact that, as the cluster is growing bigger and bigger, the energy of the cluster (per TiO_2 unit) will be decreasing and converging to that of the bulk.

It is known that the surface atoms of clusters are more reactive and imbalanced in terms of their coordination environment compared to their bulk counterparts. In the smaller clusters, the number of surface atoms is high compared to the total number of atoms in the whole cluster and hence the cluster is less stable. Once the cluster is getting bigger, the surface atoms to total atoms ratio is
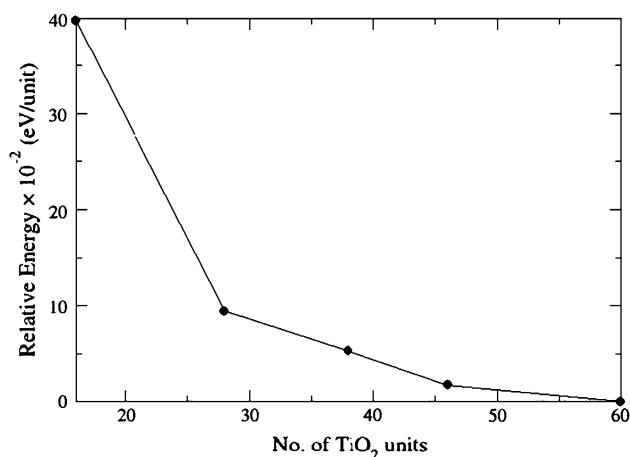

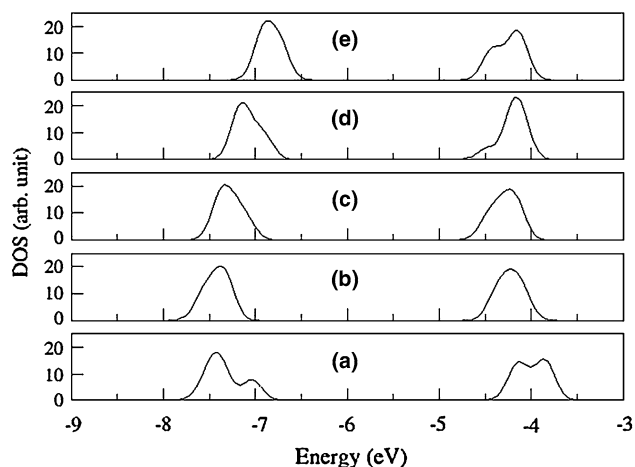**Fig. 2** Relative energy (eV/unit) of cluster with the number of TiO_2 units in the clusters

getting smaller and smaller, and the energy per unit eventually converges to the bulk value. The variation of the energy with the cluster size can also be correlated with the thickness in the z direction (i.e. normal to the surface). With increasing the thickness, the energy/TiO_2 is getting flatter and flatter. Judging from Fig. 2, we can assume that the energy is almost converged for the largest thickness of z. Thus, it can be expected that the next data point to the right of the figure would be completely converged to the ideal surface.

During the operation of the DSSC, the electrochemical potential would appear on both electrodes. The electrochemical potential of the electrode in the cell can be represented by the Fermi level of each electrode. It is already known that the cell voltage depends on the Fermi energy and hence the HOMO/LUMO of the TiO_2 electrode. In addition, the rate of the electron transfer from photoexcited dye also depends on the position of LUMO. Due to the interaction with other species, the positions of the HOMO and LUMO of TiO_2 are often shifted. Therefore, for evaluating the performance of the DSSC, it is important to know the energy state of the frontier orbitals of TiO_2. The calculated positions of the HOMO (highest occupied molecular orbital), the LUMO (lowest unoccupied molecular orbital) and the HOMO-LUMO gap are shown in Table 1. [Corresponding values from the DFT-D3 calculations are not shown or discussed since they are very similar (see Table S1).] The densities of states (DOS) for the different clusters are plotted in Fig. 3.

The HOMO-LUMO gaps for the clusters are getting narrower from smaller to bigger clusters. Although there is no direct correlation between stability and HOMO-LUMO gap, the gap is getting narrower with the size of clusters. Thus, we have found a clear trend of narrowing gaps for bigger clusters, which is in agreement with previous reports

Table 1 Calculated HOMO, LUMO and HOMO-LUMO gap for naked and adsorbed clusters (Priroda gas-phase calculations, eV)

Cluster	Adsorbate	HOMO	LUMO	Gap
48		−7.02	−4.19	2.83
	I^-	−3.05	−1.85	1.20
	I_3^-	−3.29	−2.01	1.28
84		−7.27	−4.44	2.83
	I^-	−3.86	−2.42	1.44
	I_3^-	−3.91	−2.61	1.30
114		−6.94	−4.54	2.40
	I^-	−4.24	−2.82	1.42
	I_3^-	−4.33	−3.02	1.31
138		−6.88	−4.56	2.32
	I^-	−4.54	−3.45	1.09
	I_3^-	−3.97	−2.77	1.20
180		−6.69	−4.45	2.24
	I^-	−3.76	−2.89	0.87
	I_3^-	−3.64	−2.91	0.73

Table 2 Ti–I and I–I (for I_3^-) bond distances (in Å) upon adsorption of I^- and I_3^- (Priroda gas-phase calculations)

Clusters	I^-	I_3^-		
		Ti–I1	I1–I2	I2–I3
48	2.72	2.87	3.16	2.88
48H[a]	2.80	2.81	5.55	5.05
84	2.66	2.73	3.31	2.81
114	2.66	2.85	3.10	2.99
138	2.64	2.70	3.22	2.83
180	2.67	3.03	3.06	2.90
Rutile (110)[b]	2.65			

The iodine atom closest to the Ti atom is represented as I1, and then sequentially I2 and I3

[a] Passivated cluster, see the text

[b] Periodic surface calculations using the VASP code, quoted from [36]

Fig. 3 Density of state (DOS) for the frontier orbitals of clusters with 48 (**a**), 84 (**b**), 114 (**c**), 138 (**d**) and 180 (**e**) atoms. The DOS has been obtained by broadening the discrete molecular orbitals by Gaussian functions ($\alpha = 0.1$)

[70]. The positions of the HOMO and LUMO shift positively and negatively, respectively, and hence we find smaller gaps for the larger clusters as shown in Fig. 3.

The experimental band gap for bulk anatase is around 3.0 eV. The gaps that we have obtained for our clusters are smaller than the experimental bulk values. Actually, it is an inherent problem for approximate DFT methods [71, 72] (specifically the local density and generalized gradient approximations) to underestimate the band gap of semiconductor materials. Since we are mostly interested in the (relative) shifting of frontier orbitals upon adsorption, we believe that the inaccuracy in the estimation of frontier orbitals for both bare and adsorbed clusters will be
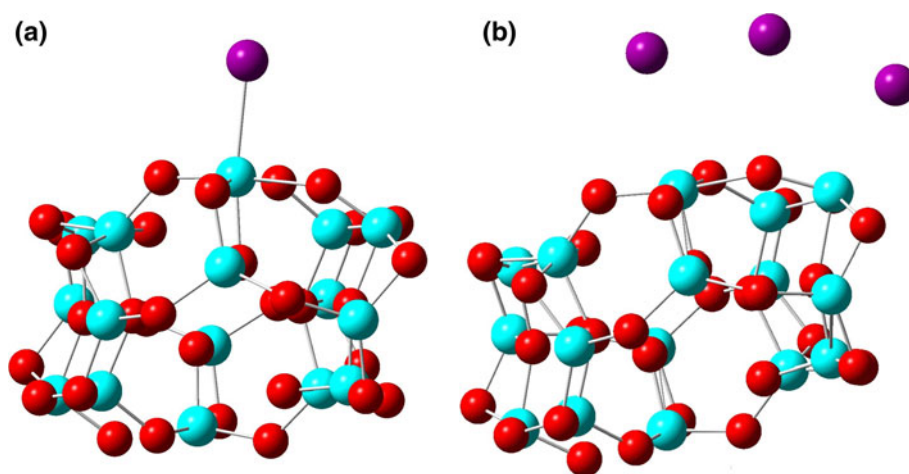
cancelled out and a reasonable shifting of frontier will be obtained.

The TiO_2 clusters have two types of active surface atoms, oxygen and titanium. Both of them are unsaturated in terms of bonding (compared to their bulk counterparts). It would be natural to expect that any species that is negatively (positively) charged would bind to the surface Ti(O) atom. Accordingly, it is observed that both I^- and I_3^- bind to the surface Ti atoms for all clusters.

The Ti–I bond distances are shown in the Table 2. The bond distance between the Ti and I atoms varies from 2.64 to 2.72 Å for I^-. This variation is due to the different chemical environments surrounding the host Ti atom. The calculated Ti–I bond distance on the rutile (110) surface is 2.65 Å, using periodic calculations [43]. The Ti–I bond distances from the cluster calculations are very close to the value calculated on the (infinite) rutile (110) surface. The T-I bond distances for I_3^- adsorption, on the other hand, are in the range of 2.70–3.03 Å. Examining the optimized structures of $TiO_2 + I_3^-$, it is observed that the triiodide decomposes to iodide and iodine species upon adsorption. The iodide adsorbs on the surface Ti atom, similar to the case of I^-. Depending on the availability, the other terminal iodine may adsorb on other surface Ti atom. The Ti–I bond distances for this iodine are longer than those for the first iodine. The middle atoms, however, do not have any surface Ti atoms to bind. Hence these iodide species are closer to the second terminal atom to balance the interactions among the three iodide species. This can be inferred from Table 2. An example for the optimized structures of I^- and I_3^- adsorption is shown in Fig. 4.

Since the adsorption of I_3^- on the surface results in a kind of decomposition of I_3^- (not completely though), the charge on the individual iodine atom is not unity as of I^-. Therefore, the electrostatic interactions between surface Ti

and the atoms of the decomposed triiodide are lower than those of Ti and I⁻. Consequently, we observe longer Ti–I bond distances in the former. This can be found in the Table 2.

The decomposition of I₃⁻ on the cluster surfaces raises the question whether surface oxygen atoms have any influence on the decomposition, as they are another reactive species at the surface. To study this phenomenon, we have modeled the cluster by saturating the dangling bonds of the surface oxygen atoms by hydrogen atoms and optimized the adsorption of I⁻ and I₃⁻ on the cluster surface (we have tested this only for the 48 cluster). For I⁻ adsorption we have, however, found almost similar structural features as previously obtained for the unsaturated cases, with only slightly lengthened Ti–I bonds (around 0.10 Å, Table 2). But for I₃⁻ adsorption, the iodine atoms further move away from each other. Both the terminal atoms adsorbed on the two surface Ti atoms and the middle iodide species move close to hydrogen atoms and thereby counter balance their negative charges by the positive charge of hydrogen, forming in effect adsorbed HI species. This is illustrated in Fig. 5. Overall, these findings show that the surface oxygen atoms have little effect on the adsorption of I⁻ and I₃⁻.

Before discussing the calculated adsorption energy, let us have a look at the bonding characteristics of the Ti–I interactions. These can be explained by Figs. 6 and 7. In Fig. 6, the total DOS and atom-projected DOS are presented. Figure 6d shows the total DOS of iodide adsorbed onto the 48 atoms cluster, whereas Fig. 6a–c represent the atom projected DOS for the O, Ti and I atoms, respectively. Looking at Fig. 6, it is observed that the 5p valence electrons of the I atom interact with the 2p of O and the 3d of Ti. This interaction is responsible for the defect-like state near the Fermi level.

Figure 7, on the other hand, represents the net electron transfer due to the adsorption of iodide on the TiO₂ cluster.
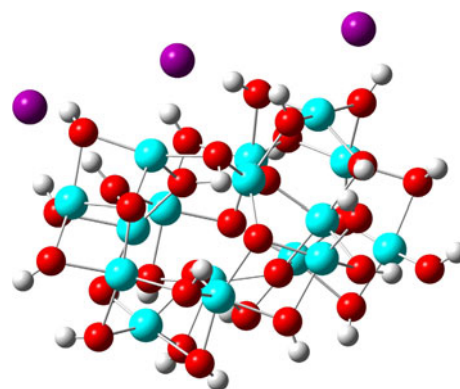

Fig. 5 Structure for adsorption of I₃⁻ on the hydrogen passivated 48 atoms cluster. The presentation is as in Fig. 4, hydrogen atoms represented as *white* spheres
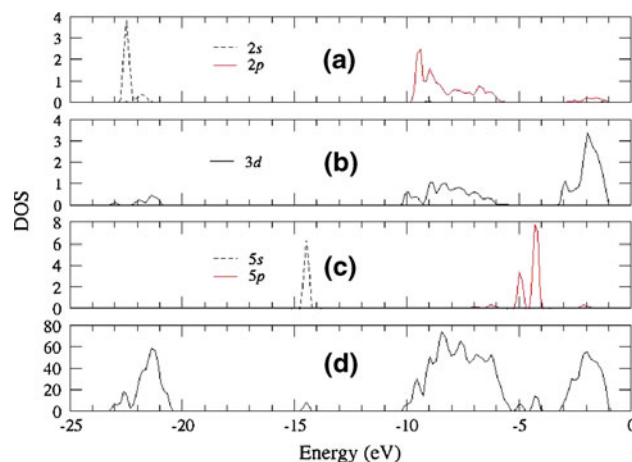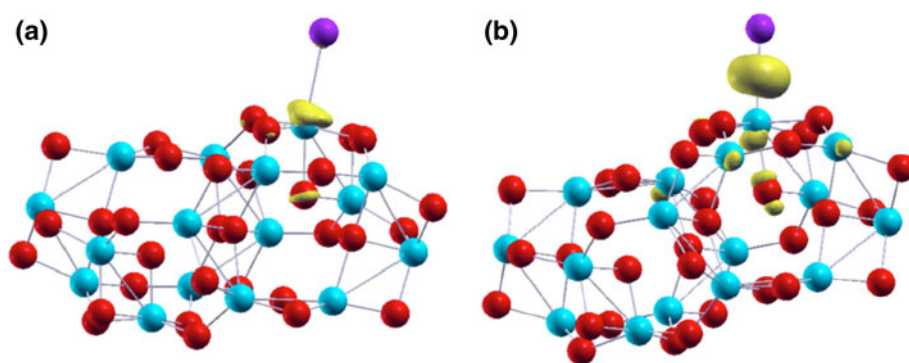

Fig. 6 The total DOS (**d**) and atom projected DOS for O (**a**), Ti (**b**) and I (**c**) of the iodide adsorbed 48 atoms cluster

The charge loss and gain (Fig. 7) are calculated as:

$$\Delta\rho = \rho(\text{TiO}_2 + \text{I}^-) - \rho(\text{TiO}_2) - \rho(\text{I}^-) \qquad (1)$$

where ρ is the total charge density. Depending on the sign of $\Delta\rho$, positive or negative, the charge gain or loss,

Fig. 7 The charge loss (**a**) and gain (**b**) due to the adsorption of iodide on the 48 atoms TiO₂ cluster. The golden color represents the charge 0.2/Å, otherwise the presentation is as in Fig. 4

respectively, is defined (Fig. 7b, a, respectively). Looking at the figure, it is observed that a substantial amount of charge from the Ti atom transfers towards the I atoms upon adsorption (7a). However, the migration of charge from Ti to I is not strong enough to form a true ionic type of bonding, rather the transferred charge is shared by both Ti and I atoms as can be seen in Fig. 7b.

The adsorption energy is calculated as:

$$\Delta E = -[E_{x-TiO_2} - E_{TiO_2} - E_x], \quad x = I^- \text{ and } I_3^- \quad (2)$$

where E is the total energy of the corresponding systems (as indicated in the subscript). The adsorption energy is defined in such a way that a higher positive value of ΔE will indicate a stronger adsorption. The adsorption energies of I^- and I_3^- are shown in the Table 3. It is clear from the Table that I^- binds much more strongly to the surface than I_3^-. The bulk Ti atoms are bonded to six neighbouring oxygen atoms. But the surface Ti atoms have less than six oxygen neighbours and hence are imbalanced in their bonding. These surface Ti atoms can easily interact with any electron-rich ligand to saturate their bonding imbalance. The valence electronic configuration of I^- is very much similar to that of oxygen (O^{2-}) in the TiO₂. Hence surface Ti binds easily to I^- and creates a bulk-like environment. This strong bond is responsible for the high adsorption energy. The same argument is also valid for I_3^-. However, we found in the previous section that I_3^- is decomposed upon adsorption, and the charges on the individual iodine species are not the same as those of I^-, resulting in a lower adsorption energy. It should be stressed that the adsorption energy of I^- on the 180 atoms clusters is somewhat lower than that of other bigger clusters (114 and 138 atoms). There are two possible explanations for such observations: (1) the bigger cluster has more local energy minima and hence it is very difficult to obtain the global energy minimum, and (2) due to the bigger size the surface atoms are of a more regular surface type and hence less reactive as opposed to those of the smaller clusters.

Including the dispersion energy, the adsorption energies are slightly higher for both I^- and I_3^- compared to their corresponding values without, Table 3. The contribution of the dispersion energy to the adsorption energy is slightly

Table 3 Adsorption energy (in eV) for I^- and I_3^- on the different clusters (Priroda gas-phase calculations)

Clusters	Dispersion correction			
	Without		With	
	I^-	I_3^-	I^-	I_3^-
48	2.31	1.55	2.43	1.75
48H	2.02	3.50	2.27	4.11
48⁻[a]	0.50	−0.05	0.69	0.22
84	3.15	1.44	3.16	1.62
114	3.89	3.31	3.96	3.65
138	4.48	3.40	4.58	3.58
180	3.42	3.75	3.45	3.96

48H is for 48 atoms hydrogen passivated cluster. The dispersion energy has been calculated with ADF

[a] Adsorption energy on the negatively charged cluster

higher for I_3^- than for I^-. This might be due to the fact that the longer bond distances in the I_3^- complexes accounted for higher dispersion energy contributions.

For the passivated cluster, the adsorption energy of I^- is slightly smaller (by around 0.30 eV) as shown in Table 3. This is probably due to steric repulsion between iodide and neighboring hydrogen atoms. The adsorption energy of I_3^-, however, is much higher (more than double) than those of naked clusters. This is due to the adsorption of the second iodide species and closeness of the middle iodide species with hydrogen. As discussed before, the process leads effectively to the formation of three adsorbed HI molecules. Although we have obtained some structural and energetic difference for the adsorption of I^- and I_3^- between passivated and naked clusters, the characteristic features for both cases (iodide adsorbed on the surface Ti atom, decomposition of I_3^- upon adsorption, etc.), however, are very similar. The inclusion of the dispersion correction to the adsorption energy provides similar trends as in the case of the naked clusters.

Looking at the positions of HOMO and LUMO according to Table 1, we observe that the positions of both

HOMO and LUMO are strongly shifted in the positive direction upon adsorption. The shifting of the positions of the HOMO in the positive direction is stronger than that of the respective LUMO and hence the HOMO-LUMO gaps for the adsorbed systems are smaller. These observations are due to the simple fact that the extra electron (charge) on I^- and I_3^- creates a defect state close to the Fermi level and hence we have found a shifted position of the HOMO. Such a shifting of frontier orbitals will have a great impact on the DSSC performance if I^- and I_3^- bind to the surface.

All calculations discussed so far have been performed in the gas phase. It might be a relevant question whether the observations would be similar when the calculations are run in solution. However, within our current computational resources and theoretical tools available, it is very difficult to run a calculation on transition metal clusters of 180 atoms in the solvent. We have, however, managed to run single point energy calculations on the gas phase optimized geometries of the 84 atoms cluster using a continuum solvation model as implemented in g03. The positions of HOMO and LUMO for both gas phase and solution phase of the 84 atoms cluster are summarized in Table 4.

The positions of the HOMO and LUMO for adsorbed clusters in the gas phase shift into the positive direction compared to those of the naked cluster. The shifts as well as the absolute values of the HOMO and LUMO positions are similar to those observed in the Priroda calculations. The HOMO and LUMO positions for the naked cluster are slightly shifted positively from gas to solution, whereas there is a strong shift in the opposite direction for adsorbed clusters. One important observation for solution calculations is that the shifting of the HOMO and LUMO from naked to adsorbed is not as drastic as we found in the gas phase. The observations of smaller shifting of frontier orbitals from naked to adsorbed clusters in solvent are due to the stabilization of excess charge on the I^- and I_3^- by the solvent.

The shifting of the HOMO can be compared with the negative shifting of the conduction band in the periodic slab study. In the adsorption of iodide on the rutile (110) surface, we have found that the negative shifting of the conduction band upon adsorption of iodide is around

0.59–0.69 eV [43]. The shifting of the HOMO of the 84 atoms clusters is 0.63 eV, which is well within the range obtained by the periodic calculations. This shifting of frontier orbitals upon adsorption of redox species might play an important role in altering the performance of DSSCs.

4 Implications for DSSCs

The photoelectrode (TiO$_2$) of DSSCs is generally covered by a monolayer of dye molecules. The photoelectron generated by the excited dye transfers to the conduction band of the photoelectrode. Thereafter, it completes the circuit and is eventually collected at the counter electrode. Now, if there is any bare part of the TiO$_2$ electrode, there is a very strong chance to adsorb the redox couple on the electrode surface. Such an opportunity of adsorption of the redox couple on the electrode has two implications for the cell performance. Firstly, the performance of the cell will be affected by shifting the position of the conduction band of the electrode. Although it has been reported [73] that a negative shifting of the conduction band enhances the performance of the cell, there must be a matching between the LUMO of the dye and the conduction band of the electrode. Shifting the conduction band above the LUMO of the dye will kill the electron transfer process and hence the cell. Secondly, the adsorption of the redox couple on the electrode surface will reduce its amount (concentration) in the electrolyte. Therefore, there might be a shortage of redox couple for the electron collection from the counter electrode and the dye regeneration process. Any of these will seriously hamper the performance of the cell.

As discussed in the introduction, Koumura et al. [34] reported a higher lifetime of the photoelectrons in the conduction band of TiO$_2$ by engineering the dye molecule. They have suggested that I_3^- needs to be blocked from coming into contact with the electrode surface. Such blocking of I_3^- from accessing the TiO$_2$ surface has also been suggested [74] as a means for suppressing dark currents. Our calculations are in agreement with these suggestions. Coming into contact with the electrode surface, I_3^- (and I^-) will bind strongly to the electrode surface and thereby the photoelectron will be lost in the processes instead of being collected at the counter electrode.

In the real DSSC, a wide variety of species is adsorbed on the surface as described, for instance, by O'Regan and Durrant [21] and it might be dangerous to try to draw a firm conclusion based on the iodide/triiodide adsorption only. However, we believe that, as a basic study on the adsorption of iodide/triiodide on the TiO$_2$ surface, our results will contribute to the understanding of possible effects on the DSSC performance due the adsorption of various species

Table 4 Positions (eV) of HOMO and LUMO of the 84 atoms cluster in the gas phase and solution (CH$_3$CN) calculated by single-point g03 calculations

Adsorbate	Gas phase		Solvation	
	HOMO	LUMO	HOMO	LUMO
	−7.32	−4.45	−6.91	−4.01
I^-	−3.93	−2.45	−6.28	−3.85
I_3^-	−4.09	−2.69	−6.10	−4.57

present in the DSSC. A complementary periodic study on the adsorption of the redox shuttle on the TiO$_2$ surface and its implication for the DSSC operation has been published elsewhere [43].

The calculations of the adsorption energy of I$^-$ and I$_3^-$ have been carried out on charge neutral TiO$_2$ clusters. However, in the actual DSSC operation, the semiconductor particles become negatively charged after accepting electrons from the excited dye molecules. Therefore, it is relevant to also study how the adsorption energies of I$^-$ and I$_3^-$ on the negatively charged TiO$_2$ are changed as compared to the neutral clusters. Consequently, we have carried out a few test calculations on the 48 atoms cluster. The adsorption energy of I$^-$ is very small for a negatively charged cluster (0.50 eV) compared to that on the neutral cluster. The adsorption energy of I$_3^-$ is −0.05 eV, which implies some repulsive interactions between I$_3^-$ and negatively charged clusters. Including the dispersion correction to the adsorption energy, the adsorption energies for I$^-$ and I$_3^-$ both become positive. That means that the adsorption of I$^-$ and I$_3^-$ is favorable even on the negatively charged clusters although the values are small compared to the neutral clusters. Still, this small adsorption energy (0.7 eV) might well be large enough to affect the DSSC performance.

5 Conclusions

Quantum-chemical calculations have been carried out on the adsorption of I$^-$ and I$_3^-$ on various TiO$_2$ clusters, noting that TiO$_2$ is used as a photoelectrode in the DSSC. Clusters sizes ranging from 48 to 180 atoms have been considered. Clusters are generated from the bulk anatase. The total energies per TiO$_2$ unit are decreasing from small to large size clusters, and it can be expected that this property will converge to the bulk value. The HOMO-LUMO gaps are getting narrower with increasing the size of clusters, and it can be expected that this will also converge to the bulk value like the total energy. This observation is in agreement with our surface calculations [43]. Our calculations reveal that both I$^-$ and I$_3^-$ are strongly adsorbed on the TiO$_2$ surface, although I$^-$ adsorbed stronger. I$_3^-$ decomposes upon adsorption due to the highly reactive surface Ti atoms. The positions of the HOMO and LUMO for the adsorbed systems shift strongly in the positive direction form their respective cluster values. Introducing the solvent stabilizes the charges on the surface atoms and iodide and thereby reduces the shifting of the HOMO and LUMO for adsorbed systems. The extent of the shifting of the HOMO is in the same range as the calculated shifting of conduction band for iodide adsorption on the rutile (110) surface. The strong adsorption of the redox

couple on a TiO$_2$ surface might affect the performance of the DSSCs both by shifting the conduction band of the photoelectrode and/or by resulting in a shortage (diminished concentration) of the available redox couple in the electrolyte solution.

References

1. Grätzel M (2001) Nature 414:338
2. Surek T (2005) J Cryst Growth 275:292
3. Yu G, Gao J, Hummelen JC, Wudl F, Heeger AJ (1995) Science 270:1789
4. Green MA (2004) Third generation photovoltaics: advanced solar energy conversion. Springer-Verlag, Berlin
5. Bisquert J, Cahen D, Hodes G, Ruhle S, Zaban A (2004) J Phys Chem B 108:8106
6. Meyer GJ (2005) Inorg Chem 44:6852
7. Peter LM (2007) J Phys Chem C 111:6601
8. Goncalves LM, Bermudez VD, Ribeiro HA, Mendes AM (2008) Energy Environ Sci 1:655
9. Grätzel M (2003) J PhotoChem Photobio C PhotoChem Rev 4:145
10. Grätzel M (2005) Inorg Chem 44:6841
11. Hamann TW, Jensen RA, Martinson ABF, Ryswyk HV, Hupp JT (2008) Energy Environ Sci 1:66
12. Bessho T, Yoneda E, Yum J-H, Guglielmi M, Tavernelli I, Imai H, Rothlisberger U, Nazeeruddin MK, Grätzel M (2009) J Am Chem Soc 131:5930
13. Mishra A, Fischer MKR, Bäuerle P (2009) Angew Chem Int Ed 48:2474
14. O'Regan B, Grätzel M (1991) Nature 353:737
15. Nazeeruddin MK, Kay A, Rodicio I, Humphry-Baker R, Muller E, Liska P, Vlachopoulos N, Grätzel M (1993) J Am Chem Soc 115:6382
16. Chiba Y, Islam A, Watanabe Y, Komiya R, Koide N, Han YL (2006) Jpn J Appl Phys, Part 2 45:L638
17. Nazeeruddin MK, DeAngelis F, Fantacci S, Selloni A, Viscardi G, Liska P, Ito E, Takeru B, Grätzel M (2005) J Am Chem Soc 127:16835
18. Grätzel M (2005) MRS Bull 30:23
19. Wang ZS, Yanagida M, Sayama K, Sugihara H (2006) Chem Mater 18:2912
20. Grätzel M (2009) Acc Chem Res 42:1788
21. O'Regan BC, Durrant JR (2009) Acc Chem Res 42:1799
22. Sauve G, Cass ME, Doig SJ, Lauermann I, Pomykal K, Lewis NS (2000) J Phys Chem B 104:3488
23. Nazeeruddin MK, Pechy P, Renouard T, Zakeeruddin SM, Humphry-Baker R, Comte P, Liska P, Cevey L, Costa E, Shklover V, Spiccia L, DEacon GB, Bignozzi CA, Grätzel M (2001) J Am Chem Soc 123:1613

24. Altobello S, Argazzi R, Caramori S, Contado C, Fre SD, Rubino P, Chone C, Larramona G, Bignozzi CA (2005) J Am Chem Soc 127:15342
25. Hoshokawa T, Ikebe T, Kikuchi R, Eguchi K (2006) Electrochim Acta 51:5286
26. Huang SY, Schlichthörl G, Nozik AJ, Grätzel M, Frank AJ (1997) J Phys Chem B 101:2576
27. Kusama H, Kurahisge M, Arakawa H (2005) J PhotoChem Photobio A. Chemistry 169:169
28. Clifford N, Palomares E, Nazeeruddin MK, Grätzel M, Durrant JR (2007) J Phys Chem C 111:6561
29. Gardner M, Giaimuccio JM, Meyer GJ (2008) J Am Chem Soc 130:17252
30. Wang ZS, Sayama K, Sugihara H (2005) J Phys Chem B 109:22449
31. Oskam G, Bergeron BV, Meyer GJ, Searson PC (2001) J Phys Chem B 105:6867
32. Hattori S, Wada Y, Yanagiad S, Fukuzumi S (2005) J Am Chem Soc 127:9648
33. Miyashita M, Sunahara K, Nishikwaw T, Uemura Y, Koumura N, Hara K, Mori A, Abe T, Suzuki E, Mori S (2008) J Am Chem Soc 130:17874
34. Koumura N, Wang ZS, Mori S, Miyashita M, Suzuki E (2006) J Am Chem Soc 128:14256
35. Hu C-H, Asaduzzaman AM, Schreckenbach G (2010) J Phys Chem C 114:15165
36. Asaduzzaman A, Schreckenbach G (2010) Phys Chem Chem Phys 12:14609
37. Dürr M, Yasuda A, Nelles G (2006) Appl Phys Lett 89:061110
38. O'Regan BC, Walley K, Juozapavivius M, Anderson A, Matar F, Ghaddar T, Zakeeruddin SM, Klein C, Durrant JR (2009) J Am Chem Soc 131:3541
39. Cramer CJ (2004) Essentials of computational chemistry: theories and models. Wiley, New York
40. Cossi M, Rega N, Giovanni S, Barone V (2003) J Comp Chem 24:669
41. Cramer CJ, Truhlar DG (1999) Chem Rev 99:2161
42. Tomasi J, Mennucci B, Cammi R (2005) Chem Rev 105:2999
43. Asaduzzaman AM, Schreckenbach G (2011) Phys Chem Chem Phys submitted
44. Delley B (2006) Mol Simul 32:117
45. Wang H-F, Liu Z-P (2009) J Phys Chem C 113:17502
46. Laikov DN (1997) Chem Phys Lett 281:151
47. Laikov DN, Ustynyuk YA (2005) Russ Chem Bull 54:820
48. Laikov DN (2005) Chem Phys Lett 416:116
49. Frisch MJ et al (2004) GAUSSIAN-03, Gaussian, Inc.
50. TURBOMOLE V6.2 2010, a development of university of Karlsruhe and Forschungszentrum Karlsruhe GmbH, 1989–2007, TURBOMOLE GmbH, since 2007, available from http://www.turbomole.com
51. ADF2008 (2008) Department of Theoretical Chemistry, Vrije University: Amsterdam, The Netherland
52. Baerends EJ, Ellis DE, Ross P (1973) Chem Phys 2:41
53. Fonseca Guerra C, Snijders JG, te Velde G, Baerends EJ (1998) Theor Chem Acc 99:391
54. Versluis L, Ziegler T (1988) J Chem Phys 88:322
55. Perdew JP, Burke K, Ernzerhof M (1996) Phys Rev Lett 77:3865
56. Asaduzzaman A, Schreckenbach G (2009) Theor Chem Acc 122:119
57. Shamov GA, Schreckenbach G, Vo T (2007) Chem Eur J 13:4932
58. Shamov GA, Schreckenbach G (2005) J Phys Chem A 109:10961
59. Gutowski KE, Dixon DA (2006) J Phys Chem A 110:8840
60. Grimme S (2006) J Comp Chem 27:1787
61. Grimme S, Anthony J, Ehrlich S, Krieg H (2010) J Chem Phys 132:154104
62. Adamo C, Barone V (1999) J Chem Phys 110:6158
63. Dyall KG (1994) J Chem Phys 100:2118
64. Dolg M, Wedig U, Stoll H, Preuss H (1987) J Chem Phys 86:866
65. Igel-Mann G, Stoll H, Preuss H (1998) Mol Phys 65:1321
66. van Lenthe E, Snijders JG, Baerends EJ (1996) J Chem Phys 105:6505
67. van Lenthe E, van Leeuwen R, Baerends EJ, Snijders JG (1996) Int J Quant Chem 57:281
68. Schäfer A, Horn H, Ahlrichs R (1992) J Chem Phys 97:2571
69. Horn M, Schwerdtfeger CF, Meagher EP (1972) Zeitschrift für Kristallographie 136:273
70. Lundqvist MJ, Nilsing M, Persson P, Lunell S (2006) Int J Quant Chem 106:3214
71. Lany S, Zunger A (2008) Phys Rev B 78:235104
72. Kümmel S, Kronik L (2008) Rev Mod Phys 80:3
73. Boschloo G, Häggman L, Hagfeldt A (2006) J Phys Chem B 110:13144
74. Nazeeruddin MK, Kay A, Rodicio I, Humphry-Baker R, Müller E, Lisaka P, Vlachopoulos N, Grätzel M (1993) J Am Chem Soc 115:6382